Bull. Nov. Comp. Center, Num. Model. in Atmosph., etc., 3 (1998), 43–56

Diagnostic calculation of the North Pacific circulation based on seasonal climatic data*

V.I. Kuzin and V.M. Moiseev

The present paper deals with the study of the North Pacific circulation and its seasonal variability according to Levitus (1994) and Hellerman, Rosenstein (1982) climatic data. The Novosibirsk Computing Center North Pacific Circulation Model based on the finite element technique was used for the calculation of the climatic currents, as well as the mass and heat fluxes. To avoid some unbalanceness of the climatic data the short-range prognostic experiments were carried out after diagnosis for each season.

The reconstruction of the velocity fields on the basis of the hydrophysical fields distributions temperature (T) and salinity (S) with the use of some mathematical relations is a classical problem of oceanography. The first of a series of the methods dealing with the solution of this problem was the dynamical method [1, 2]. This method played an important role in the estimates of currents for many regions of the World Ocean. Nevertheless, this techniques has a well-known disadvantage connected with determining the "zero" surface or the absolute velocity. In this connection any efforts in the direction of the diagnostic theory development with the use of more complete models were encouraged. Here we can refer to the computations of Sarkysian [3], Cox [4], Holland, Hirshman [5]. One of the problems arising at the diagnostic stage is unbalanceness of the climatic data, especially, in the tropical zone. Filtering of the climatic fields does not bring about the appropriate results. One of approaches which can help to overcome this problem is the "robust" technique used by Sarmiento, Bryan [6]. They introduce certain sources to the prognostic heat and salt equations to control deviations of the numerical results from the "initial" climatic data. This was also done by Fujio, Imasato [7] for the study of the deep Pacific circulation. The present study follows another approach suggested by Demin, Sarkysian [8] and later extended by Ezer, Mellor [9], who used additional adjustment calculations after the diagnostic step with the use of the prognostic primitive equations without any sources. The criteria for the adjustment period are the kinetic energy and the potential entropy behaviour. The present paper is devoted to study of the North Pacific circulation and its seasonal variations

*Supported by the Russian Foundation for Basic Research under Grant 96-05-65953.

according to the climatic data. The Novosibirsk Computing Center North Pacific Circulation Model based on the finite element technique was used for the calculations of the currents, mass and heat fluxes.

1. The model and numerical technique

Primitive equations of the ocean thermodynamics are used with the conventional approximations: Boussinesq, hydrostatics and "rigid-lid". The model is formulated in the spherical coordinates. The basin also includes the tropical zone up to 30°S. The seasonally averaged T, S climatic fields from Levitus Climatic Atlas [10] were used as the initial and the boundary conditions. The wind-stress was set at the sea surface according to Hellesman and Rosenstein [11]. At the "solid" boundaries no-flux condition for heat and salt as well as free-slip conditions for the momentum equations were used. The spatial resolution on the E-type grid is 1×2 degrees with respect to the horizontal coordinates and with 18 vertical nonuniform standard levels. The numerical technique based on the finite element approach with splitting has been developed by Kuzin [12], and applied to the North Pacific basin in the work by Kuzin and Moiseev [13].

A system of equations for the calculation of the 3D fields of velocity, temperature and salinity is prescribed in the form:

$$\frac{dU}{dt} + (f - \delta)\vec{k} \times U = -\frac{1}{\rho_0}\nabla P + \frac{\partial}{\partial z} v \frac{\partial U}{\partial z} + \vec{F}, \tag{1}$$

$$\operatorname{div} U + \frac{\partial w}{\partial z} = 0, \tag{2}$$

$$\frac{\partial P}{\partial z} = g\rho, \tag{3}$$

$$\rho = \rho(T, S), \tag{4}$$

$$\frac{d(T,S)}{dt} = \frac{\partial}{\partial z}\kappa\frac{\partial(T,S)}{\partial z} + \nabla\mu\nabla(T,S). \tag{5}$$

Equations (1)–(5) are written in the coordinates (λ, θ, z) on the sphere of the radius a; λ is longitude, $\theta = \varphi + \pi/2$, φ is latitude, z is the vertical coordinate positively directed from the surface to the center of the Earth; $U = (u, v)$ is the vector of horizontal velocity components, w is a vertical velocity component, $m = 1/a \sin\theta$, $n = 1/a$, $a = 6.38 \times 10^8$ cm, $f = -2\omega\cos\theta$ is the Coriolis parameter, $\omega = 0.73 \times 10^{-4}$ is the Earth's rotation angular speed, ρ_0 is constant standard density, ρ is density, P is pressure, $\nu = 10\,\mathrm{cm}^2/\mathrm{s}$, $\kappa = 1\ \mathrm{cm}^2/\mathrm{s}$ are the vertical eddy viscosity and diffusion coefficients respectively, $\mu = 10^6\ \mathrm{cm}^2/\mathrm{s}$ is the horizontal diffusion coefficient, T is temperature (°C), S is a salinity (‰), $\vec{k}$ is a unit vector by z-direction, $\delta = m\cos\theta u$,

$$\nabla P = \left(m\frac{\partial P}{\partial \lambda}, n\frac{\partial P}{\partial \theta}\right), \qquad \operatorname{div} U = m\left(\frac{\partial u}{\partial \lambda} + \frac{\partial}{\partial \theta}\frac{n}{m}v\right),$$

$$F = A_l\left(m\Delta U + (n^2 - m^2\cos^2\theta)U - 2m^2\cos\theta\cdot\vec{k}\times\frac{\partial U}{\partial \lambda}\right),$$

where $A_l = 2\cdot 10^6$ cm^2/s is the horizontal eddy viscosity coefficient

$$\Delta\varphi = \frac{\partial}{\partial\lambda}m\frac{\partial\varphi}{\partial\lambda} + \frac{\partial}{\partial\theta}\frac{n^2}{m}\frac{\partial\varphi}{\partial\theta}, \qquad \frac{d\varphi}{dt} = \frac{\partial\varphi}{\partial t} + mu\frac{\partial\varphi}{\partial\lambda} + nv\frac{\partial\varphi}{\partial\theta} + w\frac{\partial\varphi}{\partial z}.$$

Boundary conditions for (1)–(5) are as follows:

- at the surface:

$$z = 0: \quad w = 0, \quad \nu\frac{\partial U}{\partial z} = -\frac{\vec{\tau}}{\rho}, \quad (T,S) = (T,S)^\circ, \tag{6}$$

- at the bottom:

$$z = H(\lambda,\theta): \quad w = U\cdot\nabla H, \quad \nu\frac{\partial U}{\partial z} = -R\overline{U}, \tag{7}$$

$$\overline{U} = \frac{1}{H}\int_0^H U\,dz, \quad \frac{\partial(T,S)}{\partial z} = 0, \tag{8}$$

- at the cylindrical lateral boundaries $\Gamma = \Gamma_0 U\Gamma_1$:

a) "solid" boundary:

$$\Gamma_0: \quad \frac{\partial U\vec{l}}{\partial n} = 0, \quad \vec{U}\vec{n} = 0, \quad \frac{\partial(T,S)}{\partial n} = 0, \tag{9}$$

b) "liquid" boundary:

$$\Gamma_1: \quad U = U^0, \quad (T,S) = (T,S)^\circ. \tag{10}$$

In relations (6)–(10), $\vec{\tau}$ is the wind-stress vector, $R = 0.05$ cm/s is the bottom drag coefficient, $\vec{l}$, $\vec{n}$ are the tangent and the normal unit vectors to the boundary Γ, respectively. Index (°) marks the values, which are specified. At the initial time values, u^0, v^0, T^0, S^0 are prescribed. Solution of the system of equations (1)–(10) is found by a conventional technique [14], i. e., by separating the external (barotropic) and the internal (baroclinic) modes. This means that the velocity field U is presented as a sum $U = \overline{U} + U'$, where $\overline{U} = 1/H\int_0^H U dz$, $U' = U - \overline{U}$. Equation (5) is solved by splitting [12] with respect to the directions λ_1, θ_1 turned relative to

the axes λ, θ by the angle $\pi/4$, i.e., the angles between these axes are $(\widehat{\lambda, \lambda_1}) = (\widehat{\theta, \theta_1}) = \pi/4$.

To determine the external mode component $\overline{U}$ the integral stream function ψ is used. The equation for this function is derived from (1) vertically averaged (1) by applying the rotor operation. As a result, the integral vorticity equation in terms of the integral stream function can be presented in the form

$$\frac{\partial}{\partial t}\left(\nabla\left(\frac{1}{H}\nabla\psi\right)\right) + \nabla\left(\frac{R}{H}\nabla\psi\right) - \mathrm{rot}_z\,(\xi^*\nabla\psi)$$
$$= \mathrm{rot}_z\left(-\frac{1}{\rho_0 H}\int_0^H \nabla p\,dz\right) - \mathrm{rot}_z\frac{1}{H}\int_0^H L(U')dz + \mathrm{rot}_z\frac{\tau}{\rho_0 H} + A_l\nabla(\nabla H\xi),$$
$$H\xi = \nabla\left(\frac{1}{H}\nabla\psi\right),$$

where

$$\xi^* = \xi + \frac{f}{H}, \quad \mathrm{rot}_z\,\vec{q} = m\left(\frac{\partial q_2}{\partial\lambda} - \frac{\partial}{\partial\theta}\frac{n}{m}q_1\right), \quad \vec{q} = (q_1, q_2),$$
$$L(U') = mu\frac{\partial U'}{\partial\lambda} + nu\frac{\partial U'}{\partial\theta} + w\frac{\partial U'}{\partial z} + (f-\delta)\cdot\vec{k}\times U' -$$
$$A_l\left[m\Delta U' + (n^2 - m^2\cos^2\theta)U' - 2m^2\cos\theta\vec{k}\times\frac{\partial U'}{\partial\lambda}\right],$$

with the boundary conditions

$$\text{on } \Gamma_0: \quad \psi = 0, \ \xi = 0, \qquad \text{on } \Gamma_1: \quad \psi = \psi^0, \ \xi = \xi^0. \tag{11}$$

Equations for U' have the form

$$\frac{\partial U'}{\partial t} + L(U') = -\frac{1}{\rho_0}\left(\nabla P - \frac{1}{H}\int_0^H \nabla P\,dz\right) +$$
$$\frac{\partial}{\partial z}\nu\frac{\partial U'}{\partial z} - \frac{1}{H}\left(\nu\frac{\partial U'}{\partial z}\right)_0^H + \frac{1}{H}\int_0^H L(U')\,dz - I. \tag{12}$$

Here

$$I = mU'\frac{\partial\vec{U}}{\partial\lambda} + nv'\frac{\partial\vec{U}}{\partial\theta} + m\vec{U}U'\cos\theta.$$

The advective terms in (12) are transformed before discretization from the gradient to a special divergent form with the use of some potential function analogues:

$$\hat{u} = -\int_0^z u\,dz, \qquad \hat{v} = -\int_0^z v\,dz.$$

The vertical velocity component is determined from the relation

$$w = m\left(\frac{\partial \hat{u}}{\partial \lambda} + \frac{\partial}{\partial \theta}\frac{n}{m}\hat{v}\right).$$

According to these relations the advective terms can be written down as follows:

$$\begin{aligned} BU' &\equiv mu\frac{\partial U'}{\partial \lambda} + nv\frac{\partial U'}{\partial \theta} + w\frac{\partial U'}{\partial z} \\ &= m\left(\frac{\partial}{\partial \lambda}\hat{u}\frac{\partial U'}{\partial z} - \frac{\partial}{\partial z}\hat{u}\frac{\partial U}{\partial \lambda}\right) + m\left(\frac{\partial}{\partial \theta}\frac{n}{m}\hat{v}\frac{\partial U'}{\partial z} - \frac{\partial}{\partial z}\frac{n}{m}\hat{v}\frac{\partial U'}{\partial \theta}\right). \end{aligned}$$

The main aspects of the numerical technique are the following:

1. Momentum equations. Discretization of the equations was done on the basis of the piece-wise interpolating functions employing the "mass-lumping" technique. For the advective terms, the finite element version of the up-stream scheme was used and the implicit scheme with respect to time was applied. The pressure gradient terms as well as some part of the advective terms integrated by the vertical were treated in the explicit manner. For all other terms the Crank–Nicholson scheme was used with the block Zeidel iterative procedure.

2. Heat and Salt equations. First, the equation is split by the cross-sections of the "chess" grid, then the quasi-two-dimensional problems are discretized by piece-wise finite elements at each section with the mass and the energy conservation laws. At each time step, an additional coordinate-wise splitting is used on the basis of the Crank–Nicholson scheme which allows the construction of a completely implicit algorithm.

Discretization is done on the staggered grid for different characteristics in the manner resulting in the correct transformation of the potential energy to the kinetic energy and vice versa. As a result the model in the discrete form in adiabatic conditions conserves the first momentum (mass, heat, salt) and the total energy.

2. Numerical experiments and results

The numerical experiment has been carried out for seasons. At the initial moment the seasonal temperature, salinity fields are prescribed.

For the analysis of the results of the mass transport, the seasonal variations of three zones are selected: A (30–60°N), B (10–30°N), C (10°S–10°N). Then, the seasonal values of the integral stream function (ISF) are subtracted from the annual mean value. The results show considerable seasonal variations of maxima of the ISF for the selected zones. The peaks of variations are observed for the winter and the summer seasons. The variations of the subpolar and the subtropical gyres and the subpolar front are caused by the interaction between the Siberian High and the Aleutian Low dominating in this region. The seasonal deviations in the A- and the C-zones are positively correlated, whereas they are in the antiphase with variations in the B-zone. The value of the annual mean mass transport for the subpolar and the subtropical gyres are 20 Sv and 45 Sv, respectively. So, the Kuroshio integral mass transport varies from the summer to the winter season from the value of 63 Sv to 28 Sv.

For the diagnosis stage, the 3D momentum equations were calculated for each season during the 50-day period of the model time.

The results of the 3D velocity diagnosis are appropriate enough for extratropical zones, however for the tropical basin the circulation, meridional circulation, integral heat fluxes and some other characteristics are rather disinformative because of the inconsistency of the density field and the diagnostic model. To avoid this problem, the short-range prognostic calculations for seventy five-day periods with a primitive equation model were done for each season. This procedure, as mentioned above, is alternative to the robust technique and allows the balance of hydrophysical fields and leads to some improvement of the hydrological characteristics. Let us consider the adjustment process as well as changes it causes on the example of the autumn season. For this purpose four regions were selected: equatorial (0.5°S–0.5°N), tropical (0.5–10°N), subtropical (10–30°N) and subpolar (30–60°N). In the pictures of the kinetic energy for each region one can see that the stabilization period is very short (less than fifteen days) for subtropical and subpolar regions both for the diagnostic and adjustment modes (Figures 1 b,c). For the tropical region the period of diagnostic stabilization is slightly longer than fifteen days, whereas the adjustment needs more than thirty days (Figure 1 a). As concerns the equatorial region, the behaviour is extremely different (Figures 2 a–d). Diagnostic stabilization at the deepest levels is attained after forty days. The adjustment processes last three months. One can see that there are some oscillations during the adjustment period in this region. This process has not been analyzed in detail yet, but all the above-mentioned features are specific for each season. The results of the adjustment for the velocity fields at depths of 100 m and 5000 m are presented in Figure 3.

Now let us discuss the hydrological characteristics for the other seasons and their specific features. In Figures 4 and 5 the pictures of the winter

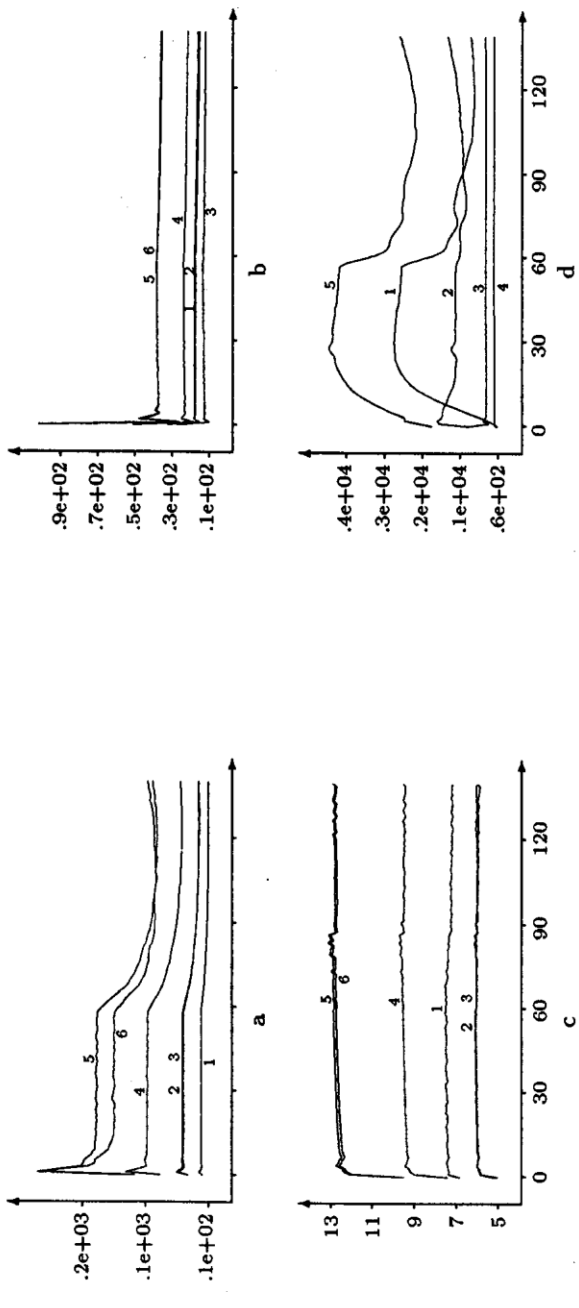

Figure 1. Graphs of the kinetic energy in the autumn in 140th day. The levels 1–6 in the regions: a – 0.5–10°N (diapason 13 ÷ 280), b – 10–30°N (13 ÷ 110), c – 30–60°N (4.5 ÷ 13). The graph d shows an average kinetic energy for the regions: 1 – 0.5°S–0.5°N, 2 – 0.5–10°N, 3 – 10–30°N, 4 – 30–60°N, 5 – all regions

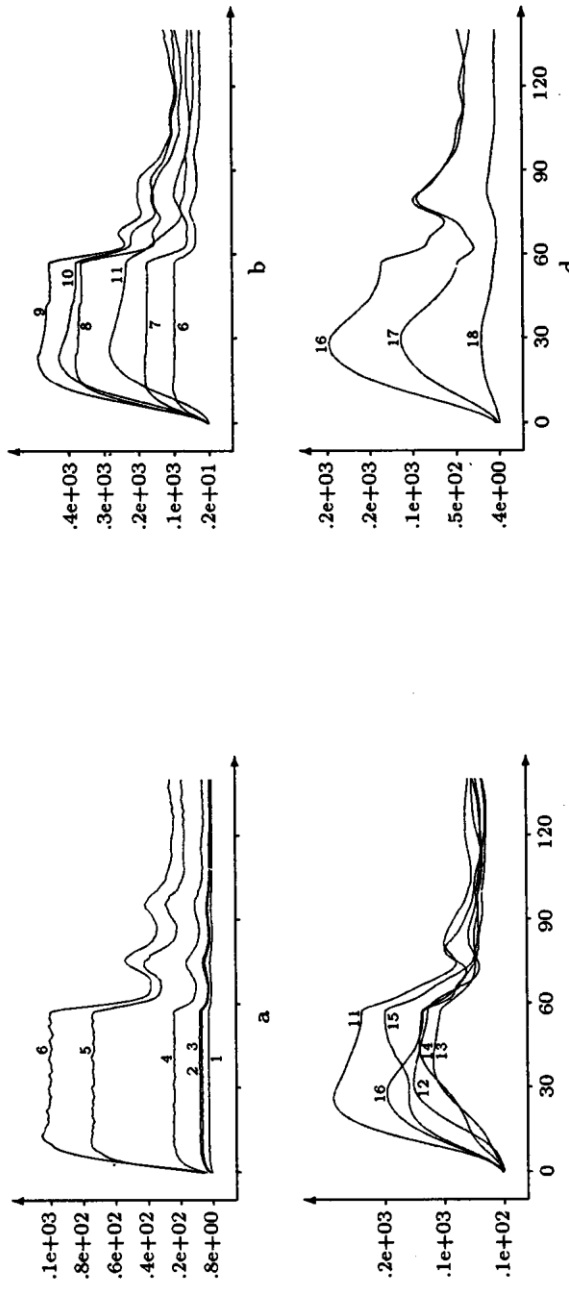

Figure 2. Graphs of the kinetic energy in the autumn for the region 0.5°S–0.5°N in 140th day:
a – levels 1–6 (0.75 ÷ 110), b – levels 6–11 (2.3 ÷ 490), c – levels 11–16 (1.6 ÷ 290), d – levels 16–18 (0.96 ÷ 200)

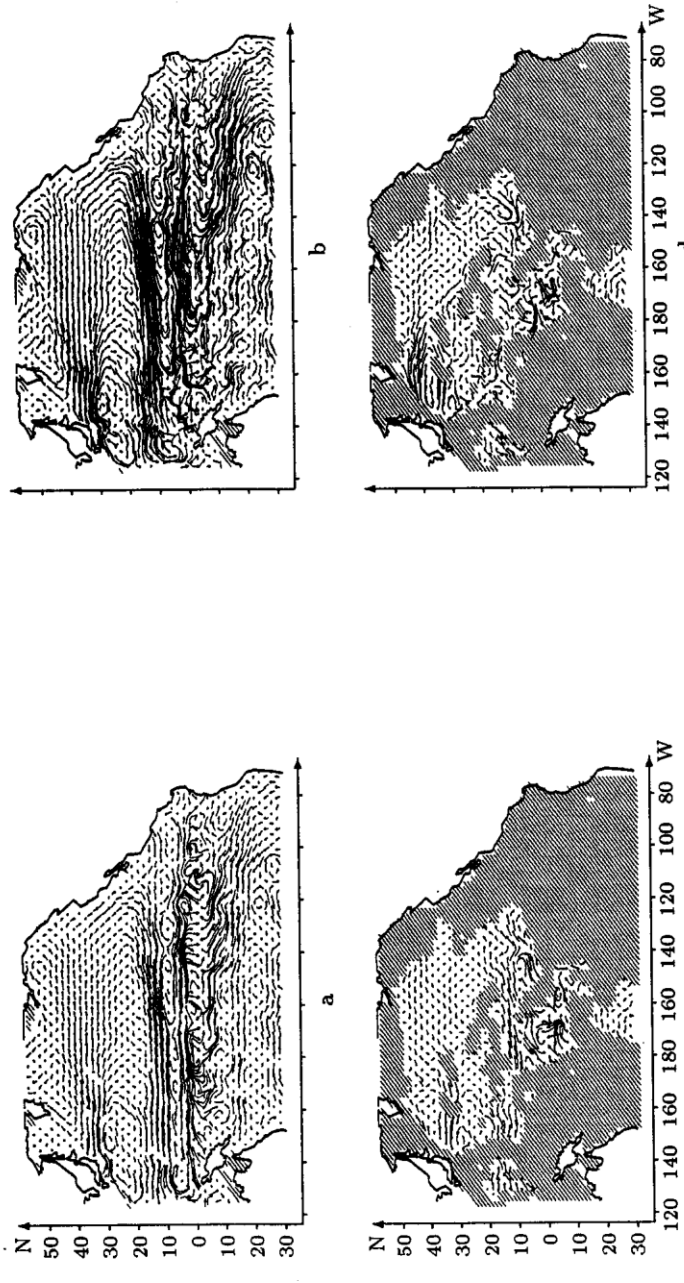

Figure 3. The velocity field in the autumn: a – the diagnose for the depth 100 m ($\max|U| = 0.84$ m/s), b – the adjustment for the depth 100 m ($\max|U| = 0.43$ m/s), c – the diagnose for the depth 5000 m ($\max|U| = 0.09$ m/s), d – the adjustment for the depth 5000 m ($\max|U| = 0.05$ m/s)

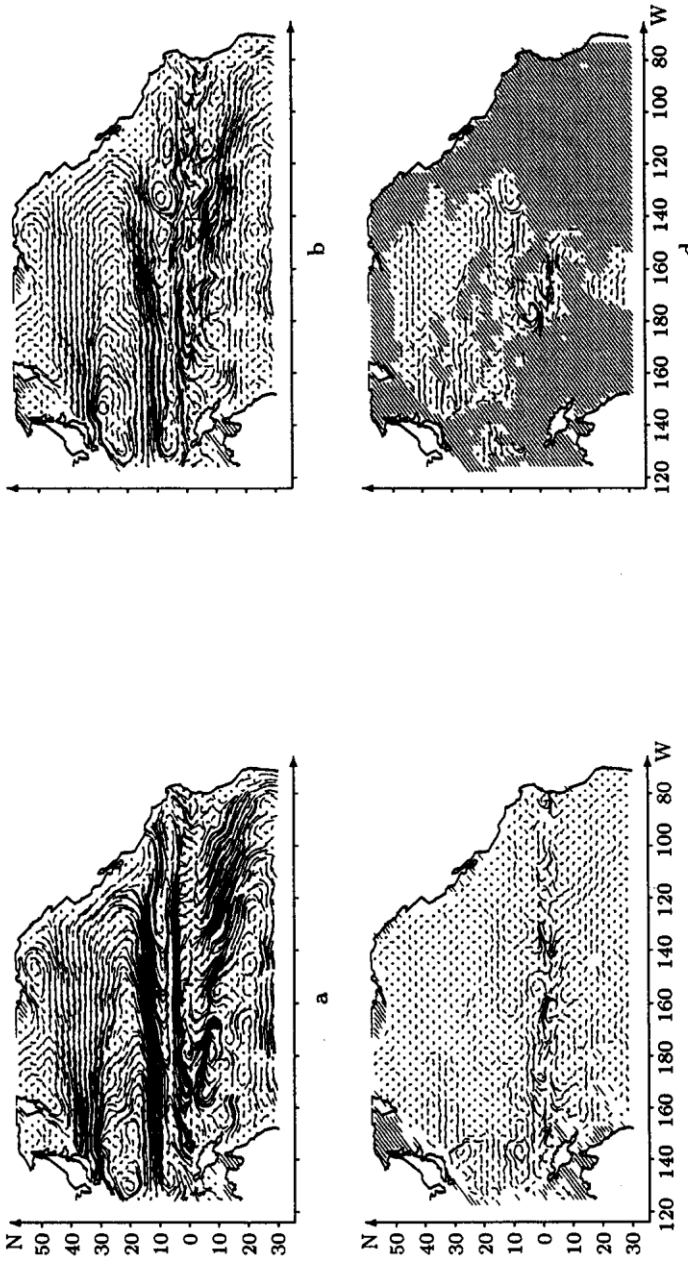

Figure 4. The adjustment of the velocity field in the winter for the depth: a – 50 m ($\max|U| = 0.32$ m/s), b – 150 m ($\max|U| = 0.39$ m/s), c – 1200 m ($\max|U| = 0.18$ m/s), d – 5000 m ($\max|U| = 0.07$ m/s)

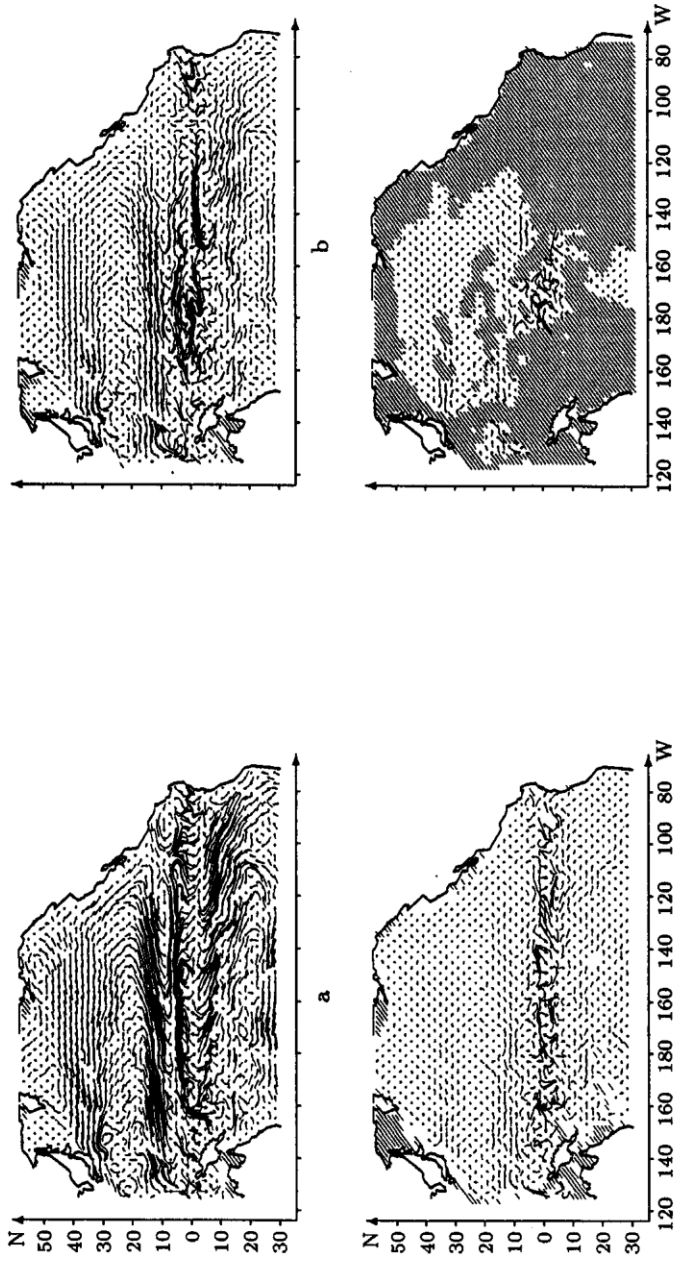

Figure 5. The adjustment of the velocity field in the summer for the depth: a – 50 m (max $|U| = 0.54$ m/s), b – 150 m (max $|U| = 0.72$ m/s), c – 1200 m (max $|U| = 0.26$ m/s), d – 5000 m (max $|U| = 0.25$ m/s)

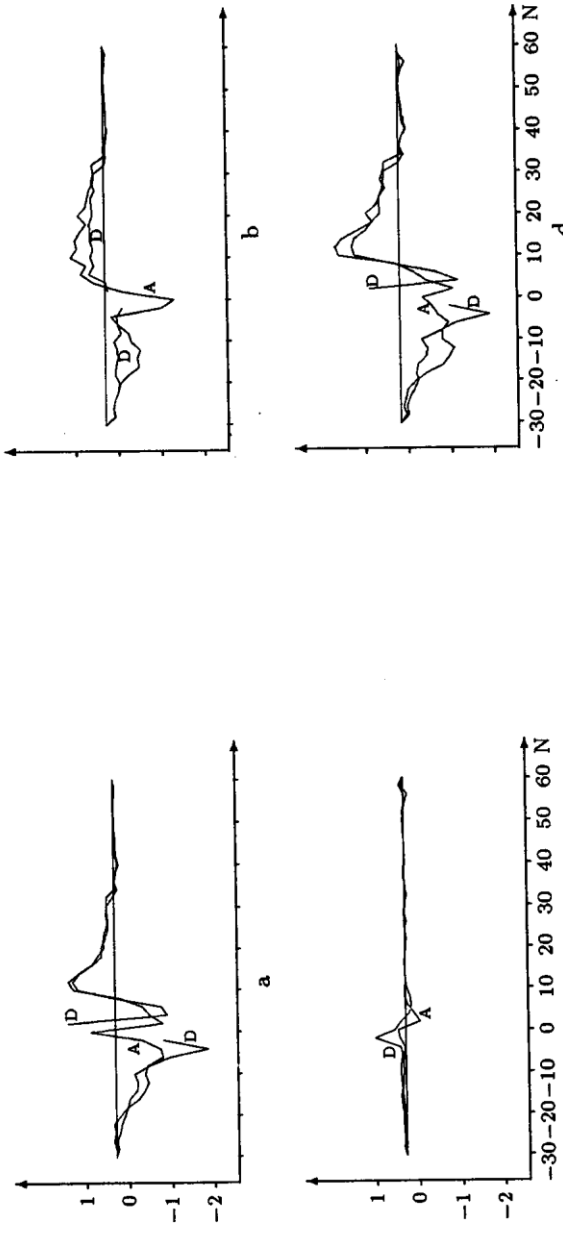

Figure 6. The graphs of the meridional heat transport (Pw) in the autumn (D – diagnose, A – adjustment) for the levels: a – 0–100 m, b – 100–900 m, c – 900–5000 m, d – 0–5000 m

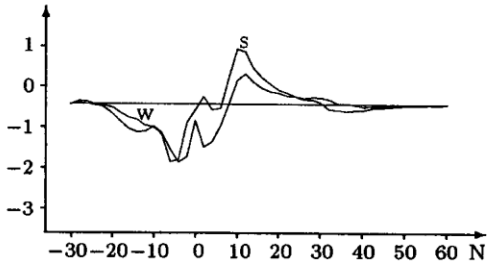

Figure 7. The adjustment of the meridional heat transport (Pw) for the levels 0–100m: W – in the winter, S – in the summer

and the summer circulations are presented at depths of 50, 150, 1200, and 5000 m. The common features of circulation in all the seasons are the presence of subpolar, subtropical and tropical systems of circulation with strong intra-tropical countercurrents and the equatorial undercurrent which begins to form. The Oyashio and the Kuroshio currents with the recirculation zones are well expressed, although are not so intensive and narrow. At the layers deeper than 1200 m there arises a system of undercurrents shifted relative to the main currents in the latitude. The main difference between the winter and the summer circulation is that for all the levels of the Northern hemisphere the currents in winter are more intensive. Finally, let us discuss such an important characteristic as the meridional heat transport which plays the key role in the atmosphere-ocean joint climatic system. Figure 6 represents transformation of the heat flux components for the autumn season during the adjustment period. The results show significant ordering and an increase of the heat flux for the layers 0–100 m and 100–900 m (see Figure 6). This is caused by improving the balance in the hydrophysical fields after adjustment. Similar processes are specific for all the other seasons. The results are in agreement with the estimates known from literature [16]. The seasonal variations presented in Figure 7 indicate to the fact that in the summer season the maximal values of the northward heat flux increased and shifted to the north being in accordance with the estimates of Levitus [15].

References

[1] Defant A. Physical Oceanography. – Oxford: Pergamon Press, 1961. – Parts I, II.

[2] Zubov H.H., Mamaev O.I. Dynamical method for sea current calculations. – Leningrad: Hydrometeoizdat, 1956 (in Russian).

[3] Sarkysian A.S. The basis for the sea currents calculation. – Leningrad: Hydrometeoizdat, 1966 (in Russian).

[4] Cox M.D. A baroclinic numerical model of the World Ocean: preliminary results // Numerical Models of Ocean Circulation. – 1975. – P. 107–120.

[5] Holland W.R., Hirchman A.D. A numerical calculation of the circulation of the North Atlantic Ocean // J. Phys. Oceanogr. – 1983. – Vol. 13. – P. 1093–1104.

[6] Sarmiento J.L., Bryan K. An ocean transport model for the North Atlantic // J. Geoph. Res. – 1982. – Vol. 87. – P. 394–408.

[7] Fujio S., Imasato N. Diagnostic Calculation for Circulation and Water Mass Movement in Deep Pacific // J. Geoph. Res.– 1991. – Vol. 96, № C1. – P. 759–774.

[8] Demin Yu.L., Sarkysian A.S. General conditions of the first stage of the numerical models intercalibration // Num. Methods and Results of the Calculations of the Atlantic Ocean Circulation. – 1992. – P. 5–12.

[9] Ezer T. and Mellor G.L. Diagnostic and prognostic calculations of the North Atlantic circulation and sea level using a sigma coordinate ocean model // J. Geoph. Res. – 1994. – Vol. 99, № C7. – P. 14159–14171.

[10] Levitus S. Climatological Atlas of the World Ocean / Environmental Res. Lab., Geophys. Fluid Dynamics Lab. – Princeton, N.J. Rockville, Md December, 1982.

[11] Hellerman S., Rosenstein M. Normal monthly wind-stress over the World Ocean with error estimates // J. Phys. Oceanogr. – 1983. – Vol. 13, № 7. – P. 1093–1104.

[12] Kuzin V.I. Finite Element Method in the Oceanic Processes Modelling. – Novosibirsk, 1985.

[13] Kuzin V.I., Moiseev V.M. North Pacific diagnostic circulation model // Bull. NCC. Ser. Num. Model. in Atmosphere, Ocean and Environment Studies. – Novosibirsk: NCC Publisher, 1995. – Iss. 1. – P. 13–30.

[14] Marchuk G.I. Numerical Solution of the Problems of the Atmosphere and Ocean Dynamics. – Leningrad: Gidrometeoizdat, 1972 (in Russian).

[15] Levitus S. Meridional Ekman Heat Fluxes for the World Ocean and Individual Ocean Basin // J. Phys. Oceanogr. – 1987. – Vol. 17. – P. 1484–1506.

[16] Talley L.D. Meridional heat transport in the Pacific Ocean // J. Phys. Oceanogr. – 1984. – Vol. 14. – P. 232–241.